Orientation Capability, Error Analysis, and Dimensional Optimization of Two Articulated Tool Heads With Parallel Kinematics

Xin-Jun Liu
Institute of Manufacturing Engineering,
Department of Precision Instruments,
Tsinghua University,
Beijing, 100084, People's Republic of China
e-mail: XinJunLiu@mail.tsinghua.edu.cn

Ilian A. Bonev[1]
Department of Automated Manufacturing Engineering,
École de Technologie Supérieure,
1100 Notre-Dame St. W.,
Montreal, Quebec, H3C 1K3, Canada
e-mail: Ilian.Bonev@etsmtl.ca

Because of the increasing demand in industry for A/B-axis tool heads, particularly in thin wall machining applications for structural aluminium aerospace components, the three-degree-of-freedom articulated tool head with parallel kinematics has become very popular. This paper addresses the dimensional optimization of two types of tool head with 3-$\underline{P}_V P_H S$ *and* 3-$\underline{P}_V RS$ *parallel kinematics (P, R, and S standing for prismatic, revolute, and spherical joint, respectively; the subscripts V and H indicating that the direction of the P joint is vertical or horizontal, and the joint symbol with underline means the joint is active) by considering their orientation capability and positioning accuracy. We first investigate the tilt angle of the spherical joint, the orientation capability, and the error of one point from the mobile platform caused by input errors. Optimization of the* 3-$\underline{P}_V P_H S$ *tool head is easy. For the* 3-$\underline{P}_V RS$ *tool head, a design space is developed to illustrate how the orientation capability and error index are related to the link lengths. An optimization process is accordingly presented. Using the optimization method introduced here, it is not difficult to find all the possible optimal solutions.* [DOI: 10.1115/1.2783255]

Keywords: parallel mechanisms, A/B-axis tool head, error analysis, optimization

1 Introduction

In order to reduce the machining time and the deformation of a workpiece, A/B-axis tool heads are now used, instead of A/C-axis tool heads, in the manufacture of structural aircraft parts with thin walls. For example, DS Technologie in Germany has developed a new machining tool head [1], the Sprint Z3, and FATRONIK in Spain has developed the Space 5H tool head [2]. The Z3 head is based on a three-degree-of-freedom (DOF) spatial parallel mechanism of type 3-PRS (P, R, and S standing for prismatic, revolute, and spherical joint, respectively), in which there is no rotation about the mobile z-axis. The Z3 head belongs to the group of so-called 3-[PP]S parallel mechanisms, which are defined as mechanisms whose three spherical joints move in vertical planes intersecting at a common line. Such a mechanism is referred to as a zero-torsion mechanism [3]. The experience with the Z3 head shows that a machine tool with such a zero-torsion tool head has advantages in terms of efficiency and accuracy. Furthermore, as we will recall from [3], a zero-torsion mechanism has a simpler kinematic model.

There is abundant literature on 3-[PP]S parallel mechanisms (even though very few authors are aware of the zero-torsion property). The 3-RPS architecture has been first analyzed by Lee and Shah [4]; two different designs of 3-PRS robots have been studied by Carretero et al. [5]; and Pond and Carretero [6]; and, finally, a 3-PCU (C and U standing for cylindrical and universal joint) has been proposed by Liu et al. [7].

Among all 3-[PP]S mechanisms, the 3-$\underline{P}_V RS$ and 3-$\underline{P}_V P_{HS}$ ones (the subscripts V and H indicating that the direction of the P joint is vertical or horizontal, and the joint symbol with underline means the joint is active) are arguably the best candidates for machining because they are best in terms of accuracy and their kinematic performances are theoretically the same on every section along the actuation direction (see [11] for details about this characteristics). In fact, the Z3 head is of 3-$\underline{P}_V RS$ type. That is why this paper focuses on the dimensional optimization of these two types of mechanisms.

Dimensional optimization is one of the most important and challenging problems in the field of parallel kinematics and is increasingly attracting the attention of researchers [8–11]. There are two issues involved: performance evaluation and dimension synthesis. Several well-defined performance indices have been extensively developed and applied in robotics. A recent study [12] reviewed the most common of these indices that have been applied in the optimum design of parallel mechanisms: the condition number [8] of the Jacobian matrix and the global conditioning index [13]. The study found serious inconsistencies when these indices are applied to parallel mechanisms with combined translational and rotational degrees of freedom, and concluded that these indices should not be used in parallel mechanisms with mixed types of degrees of freedom.

Accuracy is one of the most important performance indices in most industrial applications. Obviously, the best accuracy measure for industrial parallel kinematic machines would be the maximum output errors given input inaccuracies. The maximum error for a pose of the mechanism can be obtained either geometrically or numerically. Because of the complex kinematics of the two parallel mechanisms considered here, the error can only be calculated numerically from either the direct or the inverse kinematics. The orientation capability, i.e., the orientation workspace, of an articulated tool head seems more important than its translational capability, since most applications take advantage of the tool's rota-

[1]Corresponding author.

Contributed by the Manufacturing Engineering Division of ASME for publication in the JOURNAL OF MANUFACTURING SCIENCE AND ENGINEERING. Manuscript received November 9, 2006; final manuscript received August 3, 2007; published online February 15, 2008. Review conducted by Gloria Wiens.

tional DOFs. Therefore, for the dimensional optimization of the two articulated tool heads, accuracy and orientation capability are of interest to us here.

Many methods have been proposed for the dimensional optimization of specified mechanisms, the most common one being the objective-function-based optimal design. According to this method, an objective function with specified constraints must be established, and then a search conducted to find the result utilizing an optimization algorithm. Not only is this method time consuming, but it is difficult to reach the globally optimum target because of the nonfiniteness of the individual parameters, the antagonism of multiple criteria, and the assignment of initial values. The most serious drawback is that it provides only one solution for a design problem. This is actually a fatal one for practical design purposes, since it is impossible to predict any application in advance and to know whether a particular design is the only possible solution.

The ideal dimensional optimization method would be the performance chart (atlas), which is widely used in classical design. A performance atlas can show, globally and visually, the relationship between a performance index and the associated design parameters in a limited space [14]. Moreover, it can show how antagonistic the involved indices actually are. Compared with the result achieved by the objective-function-based method, the optimal method result is comparative and fuzzy. However, it is more flexible, because it provides not only a single solution, but all possible solutions to a design problem. This means that the designer can adjust the optimum result appropriately according to the particular design conditions he is dealing with [11].

In this paper, the method will be extended to the dimensional optimization of the two articulated tool heads. The analysis and optimization results show that the dimensional optimization of the 3-$\underline{P}_V P_H S$ tool head is very simple, and that the accuracy of the 3-$\underline{P}_V RS$ tool head can be improved by dimensional optimization.

The remainder of this paper is organized as follows. Section 2 presents the orientation description of a 3-[PP]S parallel mechanism. Section 3 describes the kinematics of the 3-$\underline{P}_V P_H S$ and 3-$\underline{P}_V RS$ tool heads. Section 4 deals with the orientation capability of these two tool heads, and Section 5 focuses on their accuracy analysis. Finally, Section 6 concerns the dimensional optimization. Conclusions are given in Section 7.

2 Orientation Description of a 3-[PP]S Parallel Mechanism

In a 3-[PP]S parallel mechanism, the centers P_1, P_2, and P_3 of the three spherical joints form an equilateral triangle (the mobile platform) and are restrained to move along the vertical planes Π_1, Π_2 and Π_3 respectively, where these planes intersect at a common line at an angle of 120 deg and are defined as restricting planes (Fig. 1).

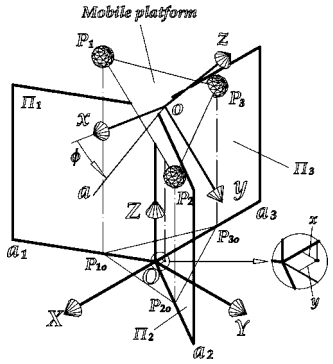

Fig. 1 Kinematic geometry of a general 3-[PP]S parallel mechanism

That the mobile platform of a 3-[PP]S parallel mechanism has two rotational DOFs and one translational DOF, is fairly common knowledge. Much less known is that any feasible orientation of the mobile platform can be obtained from the reference (home) orientation by a single rotation about a line passing through the center of the mobile platform [3]. This fact can greatly simplify the kinematic equations of such a parallel mechanism and will therefore be briefly recalled.

Let the mobile frame $\Re'$: *o-xyz* be attached at the center of the mobile platform, as shown in Fig. 1. The base frame $\Re$: *O-XYZ* is fixed to the base so that its Z-axis coincides with the line of intersection of the three restricting planes. The first problem is how to describe the orientation of the mobile platform. Most researchers have used Euler angles to do so. However, this method involves three variable angles, which is unnecessarily complex. A different method is to use the representation introduced in [3], in which only two angular parameters, referred to as the *azimuth* and *tilt* angles, are involved. The azimuth angle, denoted by ϕ, defines an *a*-axis passing through the platform center *o* and lying in the *o-xy* plane; and the tilt angle, denoted by θ, describes the swing angle about the *a*-axis. As proved in [3], any combination of azimuth and tilt angles represents a feasible orientation of the mobile platform of a 3-[PP]S mechanism and any feasible orientation can be represented by a pair of azimuth and tilt angles.

Thus, the corresponding rotation matrix $\boldsymbol{R}_a(\theta)$ can be written as

$$\boldsymbol{R}_a(\theta)=\begin{bmatrix} \cos^2\phi(1-\cos\theta)+\cos\theta & \sin\phi\cos\phi(1-\cos\theta) & \sin\phi\sin\theta \\ \sin\phi\cos\phi(1-\cos\theta) & \sin^2\phi(1-\cos\theta)+\cos\theta & -\cos\phi\sin\theta \\ -\sin\phi\sin\theta & \cos\phi\sin\theta & \cos\theta \end{bmatrix} \tag{1}$$

where ϕ is measured between the *x*-axis (not the *X*-axis) and the *a*-axis. Since the line defined by ϕ is the same as that defined by 180 deg$+\phi$, we impose $-90\ \text{deg} \le \phi \le 90\ \text{deg}$.

In the mobile frame *o-xyz*, vectors $\boldsymbol{p}_i'$ $(i=1,2,3)$, which are defined as the position vectors of points P_i, can be written as

$$\boldsymbol{p}_i' = \begin{bmatrix} r\cos\psi_i & r\sin\psi_i & 0 \end{bmatrix}^{\mathrm{T}}, \quad i=1,2,3 \tag{2}$$

in which $\psi_i=(2i-3)\pi/3$ and r is the radius of the mobile platform, i.e., the distance from points P_i to the origin *o*.

Unfortunately, when the mobile platform of a 3-[PP]S mechanism tilts in any direction, the center of the mobile platform (point *o*) does not stay on the *Z*-axis. Thus, there are so-called parasitic motions along the *X* and *Y* axes, as shown in Fig. 1. They are

$$x = d_x = -\frac{1}{2} r\cos 2\phi(1-\cos\theta) \tag{3}$$

$$y = -P_{3y} = \frac{1}{2} r\sin 2\phi(1-\cos\theta) \tag{4}$$

which clearly indicate that the center of the mobile platform shifts away from the *Z*-axis when the platform tilts. The offset, denoted by ν, can be written as

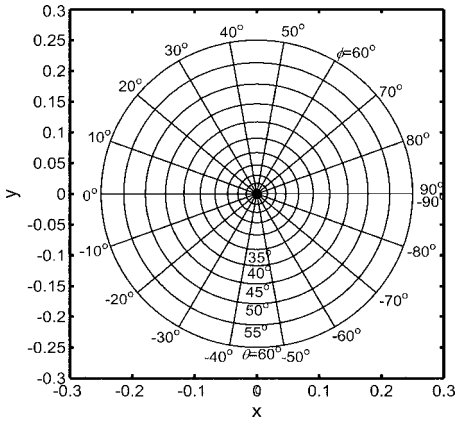

Fig. 2 Horizontal offset as a function of the orientation of a 3-[PP]S parallel mechanism

$$\nu = \sqrt{x^2 + y^2} = \frac{1}{2} r(1 - \cos\theta) \tag{5}$$

with the direction defined by φ

$$\varphi = \tan^{-1}\left(\frac{y}{x}\right) = \begin{cases} \pi - 2\phi, & \frac{\pi}{2} \geq \phi \geq \frac{\pi}{4} \\ -2\phi, & \frac{\pi}{4} > \phi > -\frac{\pi}{4} \\ -\pi - 2\phi, & -\frac{\pi}{4} \geq \phi \geq -\frac{\pi}{2} \end{cases} \tag{6}$$

To understand the coupling between position and orientation more clearly, we show in Fig. 2 the curves for x and y for constant ϕ or θ. From Eqs. (3) and (4), we can see that $x(\phi,\theta)=x(\phi,-\theta)$ and $y(\phi,\theta)=y(\phi,-\theta)$. Therefore, Fig. 2 illustrates not only the curves when $\theta \geq 0$, but also those when $\theta \leq 0$.

Thus, by using only three parameters (z, ϕ, θ), we can completely represent the pose of the mobile platform of a general 3-[PP]S parallel mechanism. Moreover, having identified the exact nature of the interdependence of the orientation parameters, the analysis of any 3-[PP]S parallel mechanism will be much simpler.

3 Kinematics of the Two Articulated Tool Heads

As shown in Fig. 3(a), the 3-$\underline{P}_V P_H S$ tool head comprises three identical legs, each consisting of one spherical joint and two prismatic joints. In each leg, the prismatic joint attached to the base is vertical and actuated, while the other prismatic joint is horizontal and passive. The 3-$\underline{P}_V RS$ tool head shown in Fig. 3(b) comprises three identical legs, each consisting of a spherical joint, a revolute joint, and a prismatic joint. In each leg, the prismatic joint is vertical and actuated. Finally, in each design, the three legs remain in three vertical planes, called the restricting planes, which intersect at a common line at an angle of 120 deg, and the centers of the spherical joints form an equilateral triangle.

Referring again to Fig. 3, let R be the distance from point O to the actuated vertical prismatic joint; r is the radius of the mobile platform, i.e., $r=|oP_i|$ ($i=1,2,3$), and L is the leg length of the 3-P_VRS mechanism. If the pose (ϕ,θ,z) of the mobile platform is given, then the position vector of each point P_i ($i=1,2,3$) in the base frame is defined as

$$\boldsymbol{p}_{i\Re} = \begin{bmatrix} x_{i\Re} & y_{i\Re} & z_{i\Re} \end{bmatrix}^{\mathrm{T}} = \boldsymbol{R}_a(\theta)\boldsymbol{p}_i' + \boldsymbol{c}_{\Re}, \quad i = 1,2,3 \tag{7}$$

where $\boldsymbol{R}_a(\theta)$ is the rotation matrix defined in Eq. (1); $\boldsymbol{p}_i'$ is the position vector of P_i in the mobile frame as expressed in Eq. (2); $\boldsymbol{c}_{\Re}=[x \quad y \quad z]^{\mathrm{T}}$ is the position vector of the platform center o expressed in the base frame; and x and y are the parasitic motions given by Eqs. (3) and (4).

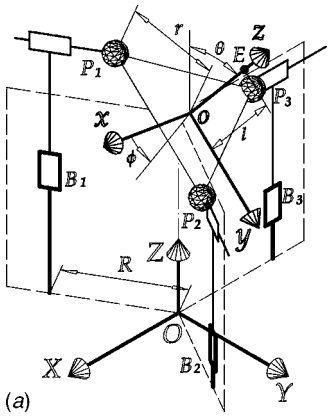

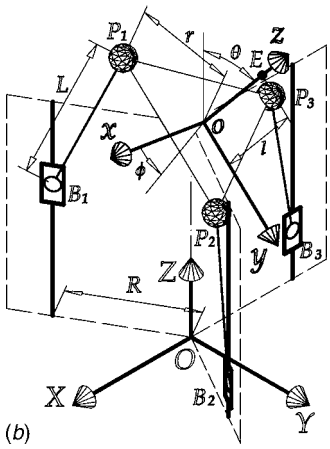

Fig. 3 Schematics of the two articulated tool heads: (*a*) with 3-$\underline{P}_V P_H S$ parallel kinematics and (*b*) with 3-$\underline{P}_V RS$ parallel kinematics

For the 3-$\underline{P}_V P_H S$ mechanism, supposing that the inputs of the legs are ρ_{i_PPS} ($i=1,2,3$), the inverse kinematic problem of the mechanism can be written as

$$\rho_{i\_\mathrm{PPS}} = z_{i\Re} \tag{8}$$

where $z_{i\Re}$ can be obtained from Eq. (7) when the pose (ϕ,θ,z) of the mobile platform is given. Then, we have

$$\rho_{1\_\mathrm{PPS}} = -\tfrac{1}{2} r \sin\theta(\sin\phi + \sqrt{3}\cos\phi) + z \tag{9}$$

$$\rho_{2\_\mathrm{PPS}} = -\tfrac{1}{2} r \sin\theta(\sin\phi - \sqrt{3}\cos\phi) + z \tag{10}$$

$$\rho_{3\_\mathrm{PPS}} = r \sin\phi \sin\theta + z \tag{11}$$

We can see that there is only one geometric parameter, i.e., r, in the kinematics of the mechanism. What is more, the inverse kinematic solution is unique.

For the 3-$\underline{P}_V RS$ mechanism, vectors $\boldsymbol{b}_{i\Re}$ ($i=1,2,3$), which are defined as the position vectors of points B_i, can be expressed in the base frame as

$$\boldsymbol{b}_{i\Re} = [R\cos\psi_i \; R\sin\psi_i \; \rho_{i\_\mathrm{PRS}}]^{\mathrm{T}}, \quad i = 1,2,3 \tag{12}$$

where ρ_{i_PRS} constitutes the Z-coordinates of points B_i. The inverse kinematic problem of the mechanism can be solved by writing the following equations:

$$|\boldsymbol{p}_{i\Re}\boldsymbol{b}_{i\Re}| = L \tag{13}$$

Substituting Eqs. (7) and (12) into Eq. (13), we have

$$\rho_{i\_\mathrm{PRS}} = \tfrac{1}{2}(-D_i \pm \sqrt{D_i^2 - 4F_i}) \tag{14}$$

in which

$$D_1 = r\sin\theta(\sin\phi + \sqrt{3}\cos\phi) - 2z$$

$$F_1 = [r(1-\cos\theta)\sin\phi(\sin\phi - \sqrt{3}\cos\phi) + r\cos\theta - R]^2 + \left[z - \tfrac{1}{2}r\sin\theta(\sin\phi + \sqrt{3}\cos\phi)\right]^2 - L^2$$

$$D_2 = r\sin\theta(\sin\phi - \sqrt{3}\cos\phi) - 2z$$

$$F_2 = [r(1-\cos\theta)\sin\phi(\sin\phi + \sqrt{3}\cos\phi) + r\cos\theta - R]^2 + \left[z - \tfrac{1}{2}r\sin\theta(\sin\phi - \sqrt{3}\cos\phi)\right]^2 - L^2$$

$$D_3 = -2(r\sin\phi\sin\theta + z)$$

$$F_3 = \left[R - \tfrac{1}{2}r(1-\cos\theta)(3 - 4\sin^2\phi) - r\cos\theta\right]^2 + (r\sin\phi\sin\theta + z)^2 - L^2$$

From Eq. (14), we can see that, for a given pose (ϕ, θ, z), there are at most eight inverse kinematic solutions, corresponding to eight working modes of the mechanism. We are concerned here with the working mode shown in Fig. 3(*b*), which can be reached when the "±" sign in Eq. (14) is "–" for all three legs.

Referring to Fig. 3, let E be a point on the mobile z-axis (the tool tip), in each of the two tool heads, such that the distance between points E and o is l. After a rotation at an angle θ about an a-axis (defined by an angle ϕ from the x-axis to the a-axis), the position vector $\boldsymbol{e}$ of point E, expressed in the base frame is

$$\boldsymbol{e} = [x_E\ y_E\ z_E]^{\mathrm{T}} = \boldsymbol{R}_a(\theta)[0\ 0\ l]^{\mathrm{T}} + \boldsymbol{c}_{\mathfrak{R}} \tag{15}$$

where

$$\begin{cases} x_E = l\sin\phi\sin\theta - \tfrac{1}{2}r\cos 2\phi(1-\cos\theta) \\ y_E = \tfrac{1}{2}r\sin 2\phi(1-\cos\theta) - l\cos\phi\sin\theta \\ z_E = l\cos\theta + z \end{cases} \tag{16}$$

4 Orientation Capability Analysis

4.1 Tilt Angle of a Spherical Joint. In this paper, orientation capability is defined as the maximum tilt angle θ for a given azimuth angle ϕ. In each of the two tool heads, there are three spherical joints. It is well known that a spherical joint has a limited tilt angle but unlimited self-rotation. For this reason, we are only concerned with the tilt angle of each spherical joint. This angle restricts the orientation capability of the whole mechanism. When the orientation parameters ϕ and θ of the mechanism are specified, the tilt angle of each spherical joint can be obtained. The tilt angle is actually determined by the orientation of lines oP_i and P_iB_i. Most often, instead of using ball joints, spherical joints having the wrist structure shown in Fig. 4(*a*) are chosen, where the w-axis is defined as the self-rotation axis, and the tilt angle is relative to the rotation angles about the v and u axes, which are referred to as the *pitch* and *yaw* angles, respectively, denoted here by α_v and α_u.

For the third leg of the 3-$\underline{\mathrm{P}}_{\mathrm{V}}\mathrm{P}_{\mathrm{H}}$S mechanism, the two angles are illustrated in Fig. 4(*b*), where points o_o and P_{3o} are the projections of points o and P_3 in the O-XY plane. Because the orientation of the w-axis remains constant, the pitch and yaw angles are

$$\alpha_v = \tan^{-1}\left(\frac{z_{3\mathfrak{R}} - z}{|o_oP_{3o}|}\right) = \tan^{-1}\left[\frac{\sin\phi\sin\theta}{\sqrt{1-\sin^2\phi\sin^2\theta}}\right] \tag{17}$$

$$\alpha_u = \tan^{-1}\left(\frac{y}{x - x_{3\mathfrak{R}}}\right) = \tan^{-1}\left[\frac{\sin\phi\cos\phi(1-\cos\theta)}{\cos^2\phi + \sin^2\phi\cos\theta}\right] \tag{18}$$

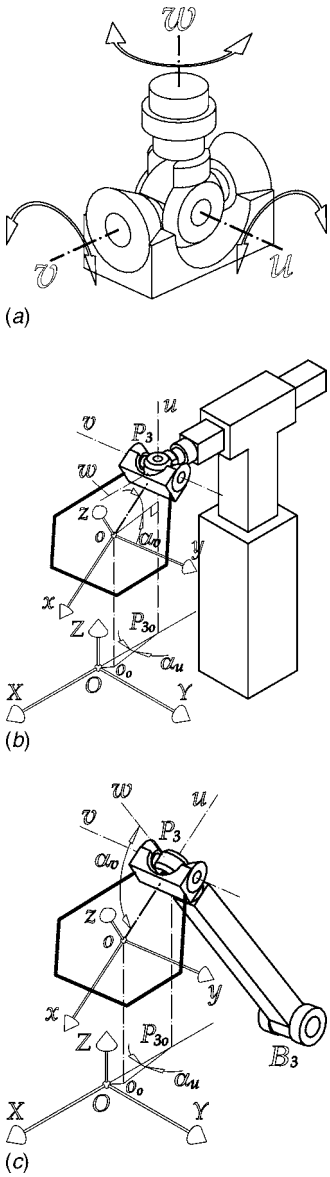

Fig. 4 Tilt angle of a spherical joint: (*a*) a type of spherical joint, (*b*) this joint in a 3-$\underline{\mathrm{P}}_{\mathrm{V}}\mathrm{P}_{\mathrm{H}}$S mechanism, and (*c*) this joint in a 3-$\underline{\mathrm{P}}_{\mathrm{V}}$RS mechanism

The above equations show that the pitch and yaw angles are independent of the parameters r and z. Figure 5(*a*) illustrates the corresponding angles of the spherical joint at P_3 as function of the orientation of the platform of a 3-$\underline{\mathrm{P}}_{\mathrm{V}}\mathrm{P}_{\mathrm{H}}$S mechanism. It shows that, at any orientation, the pitch angle is never less than the yaw angle. If the tilt angle θ belongs to [−60 deg, 60 deg], the maximum yaw angle is smaller than 20 deg and the maximum pitch angle is equal to the maximum tilt angle of the mobile platform.

As shown in Fig. 4(*c*), since the orientation of the w-axis in the spherical joint of the 3-$\underline{\mathrm{P}}_{\mathrm{V}}$RS mechanism varies, the pitch angle α_v from the w-axis can no longer be calculated by Eq. (17), while the yaw angle α_u can be still obtained using Eq. (18). For the spherical joint in the third leg of the 3-$\underline{\mathrm{P}}_{\mathrm{V}}$RS mechanism, angle α_v can be expressed as

$$\alpha_v = \pi - \cos^{-1}\left(\frac{|oP_3|^2 + |P_3B_3|^2 - |oB_3|^2}{2|oP_3||P_3B_3|}\right) \tag{19}$$

where α_v is independent of z. Since the spherical joint is usually not pitched from zero, the angle given in Eq. (19) is not the

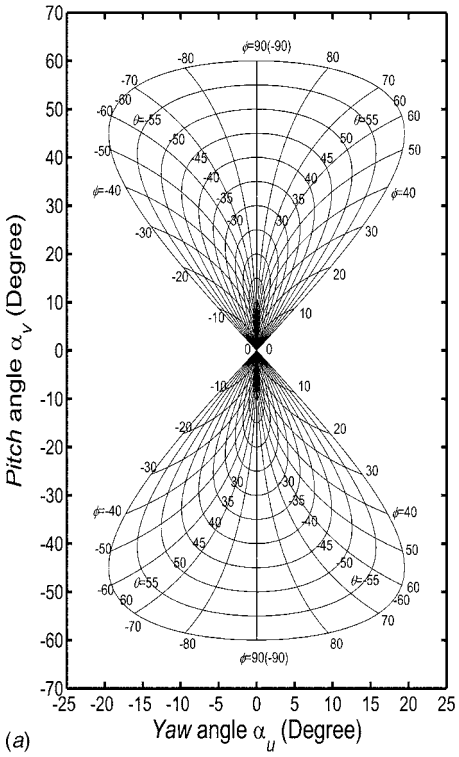

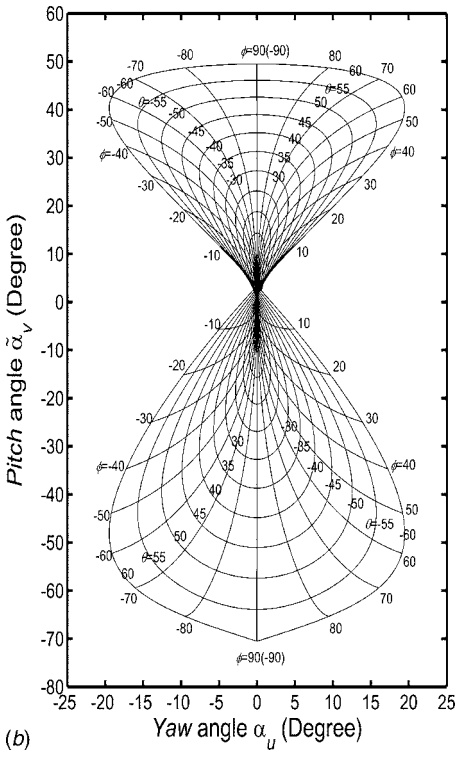

Fig. 5 Relationship between the tilt angle of a spherical joint and the orientation of the mobile platform: (*a*) for a 3-$\underline{P}_V P_H S$ tool head and (*b*) for a 3-$\underline{P}_V RS$ tool head

absolute pitch angle of the spherical joint. In this paper, the absolute pitch angle is defined as the relative angle between the current orientation and the reference orientation ($\theta=0$). At $\theta=0$, the pitch angle is denoted by α_{vo}. Then, the absolute pitch angle of the spherical joint will be $\tilde{\alpha}_v=\alpha_v-\alpha_{vo}$.

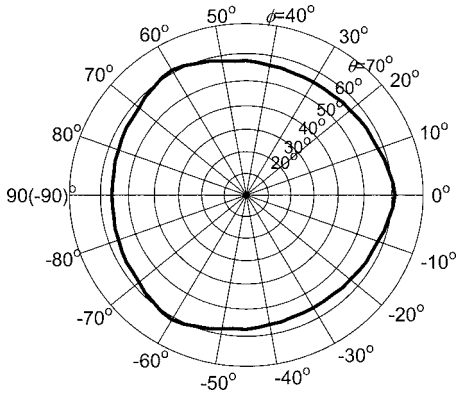

Fig. 6 Orientation capability of a 3-$\underline{P}_V RS$ tool head as limited by singularities only

For example, if $R=2.5$, $r=1.0$, $L=4.5$, $\alpha_{vo}=70$ deg, and $\theta\in[-60\text{ deg},\ 60\text{ deg}]$, then the angles $\tilde{\alpha}_v$ and α_u for a constant orientation (ϕ,θ) are as illustrated in Fig. 5(*b*), which shows that, in a 3-$\underline{P}_V RS$ mechanism, just as is the case in a 3-$\underline{P}_V P_H S$ mechanism, the pitch angle is larger than the yaw angle and reaches its maximum when $\phi=90$ deg. From Figs. 5(*a*) and 5(*b*), we see that, unlike the case of a 3-$\underline{P}_V P_H S$ mechanism, the pitch and yaw angles of a 3-$\underline{P}_V RS$ mechanism are not symmetrical with respect to $\theta=0$. For this reason, in assembling a 3-$\underline{P}_V RS$ mechanism, the spherical joint should be mounted at an inclination to avoid exceeding its pitch limits.

4.2 Orientation Capability of the 3-$\underline{P}_V P_H S$ Tool Head. As shown in Fig. 5(*a*), for the third leg of this tool head, the pitch angle reaches its maximum when $\phi=90$ deg. Using the structure shown in Fig. 4(*a*), the pitch capability of such a spherical joint can be as high as ± 90 deg and the yaw capability nearly ± 45 deg. Therefore, the orientation capability of the mobile platform of a 3-$\underline{P}_V P_H S$ mechanism is actually determined by the pitch angle of the spherical joint, and it can be as high as ± 90 deg. However, the mechanism is in a singularity at $\alpha_v=\pm 90$ deg. Besides, a tilting capability in the ± 60 deg range is high enough for machining applications.

4.3 Orientation Capability of the 3-$\underline{P}_V RS$ Tool Head. It is worth noting that, although Fig. 5(*b*) shows that the mobile platform can reach an orientation capability of $[-60\text{ deg},\ 60\text{ deg}]$, not all 3-$\underline{P}_V RS$ mechanisms have such a capability. Indeed, the orientation capability also depends on the mechanism singularities.

While the 3-$\underline{P}_V P_H S$ mechanism has no singularities for tilt angles of less than 90 deg, the 3-$\underline{P}_V RS$ mechanism has two types of singularity. The first type occurs when a leg P_iB_i is normal to the direction of actuator i, which in our case is along the Z-axis, whereas the second type occurs when a leg lies in the plane of the mobile platform.

In the application of a 3-$\underline{P}_V RS$ tool head, we usually expect its tilt angle limits to be symmetrical with respect to its reference orientation ($\theta=0$), for a given a-axis (specified by ϕ). For example, we usually say that the tool head can tilt ± 40 deg, but not +30 deg and −50 deg, with respect to any a-axis. Here, for a given ϕ, the tilt angle is denoted by θ_P when the mobile platform is in a first type of singularity, and it is referred to as θ_N when the mobile platform is in a second type of singularity. Therefore, in this paper, the orientation capability for a specified ϕ of a 3-$\underline{P}_V RS$ mechanism is defined as the absolute value of the smaller of θ_P and θ_N.Then, if the orientation capability for a specified ϕ is 45 deg, we say that the mobile platform can tilt ± 45 deg about the a-axis.

For example, the orientation capability of a 3-$\underline{P}_V RS$ mechanism with $R=2.5$, $r=1.0$, and $L=4.5$ is shown in Fig. 6, from which we

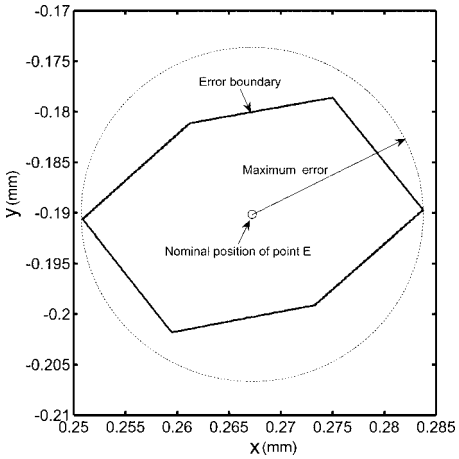

Fig. 7 Error region in the *o-xy* plane for a given pose of the 3-$\underline{P}_V P_H S$ tool head

can see that the capability reaches its maximum of ~61 deg when $\phi=0$, −60 deg and 60 deg, and its minimum of ~56 deg when $\phi=30$ deg, −30 deg, and ±90 deg. It is worth noting that the orientation capability of the 3-$\underline{P}_V$RS mechanism is independent of the z coordinate.

Thus, from Fig. 6, we can pinpoint the largest tilt that can be accomplished in any direction (any ϕ) without reaching a singularity, which for this example is ~56 deg. Of course, the tilt should be further limited because the mechanism performance deteriorates significantly when a singularity is close. How close to a singularity can the mechanism safely operate is a question that requires further analyses that are not the object of this paper. Let us assume that in this example, we may operate safely within a 50 deg tilt.

Having defined the maximal singularity-free orientation capability, we should find the corresponding required characteristics for the spherical joints. Figure 5(*b*) shows that we should be only concerned about the pitch angle $\tilde{\alpha}_v$, which reaches its maximum value of $\tilde{\alpha}_v=42.57$ deg when $\theta=50$ deg (−50 deg) and $\phi=90$ deg (−90 deg) and its minimum value of $\tilde{\alpha}_v=-57.43$ deg when $\theta=50$ deg (−50 deg) and $\phi=-90$ deg (90 deg).

5 Error/Accuracy Analysis

It is obvious that the presence of input errors will mean that the mobile platform will be undesirably offset from its nominal pose, as will be the point E. Supposing that, at a given nominal pose (ϕ,θ,z), the nominal position of point E is at $E_N(x_E,y_E,z_E)$, the real position of point E is actually at $E_N^e(x'_E,y'_E,z'_E)$ because of the input errors. Since the real position of point E is near its nominal position, in order to show the shape of the error region, defined by the possible real positions of the point for the input range $[\rho_i-\varepsilon,\rho_i+\varepsilon]$ $(i=1,2,3)$, we can project these positions to the mobile platform plane, i.e., the *o-xy* plane, when at its nominal pose. The projection equation is

$$(x''_E\ y''_E\ z''_E)^{\mathrm{T}}=\boldsymbol{R}_a^{-1}(\theta)[(x'_E\ y'_E\ z'_E)^{\mathrm{T}}-(x\ y\ z)^{\mathrm{T}}] \tag{20}$$

where $(x''_E\ y''_E)^{\mathrm{T}}$ is the position vector of the projection of point E_N^e in the *o-xy* plane and $(x\ y\ z)^{\mathrm{T}}$ is the platform nominal position vector. For example, if $\phi=50$ deg, $\theta=20$ deg, $\varepsilon=10$ μm, $l=1$ mm, and $z=0$, the error region for a 3-$\underline{P}_V P_H S$ tool head is shown in Fig. 7.

The distance from the nominal position to the real position is denoted as $|E_N E_N^e|$. The maximum distance, referred to as E_e, is defined as the maximum error at a given nominal pose.

To obtain numerically the value of E_e for a given nominal pose (ϕ,θ,z), we must first calculate the nominal position coordinates

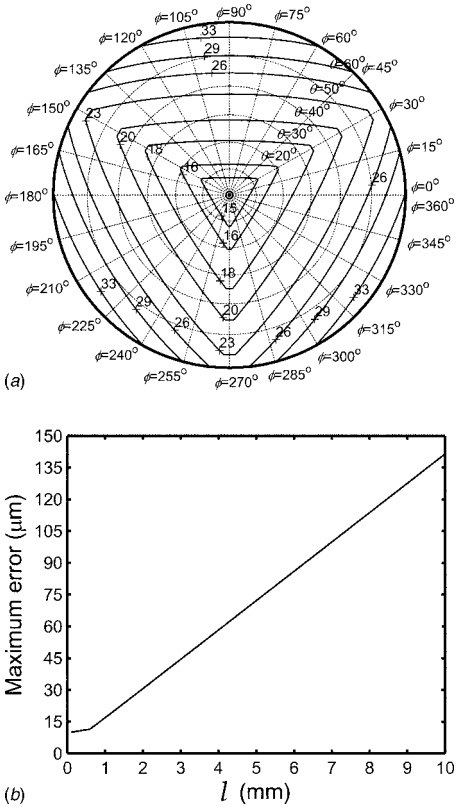

Fig. 8 Maximum error (in micron) versus platform orientation and the length *l* for a 3-$\underline{P}_V P_H S$ tool head: (*a*) maximum error for different orientation for *l*=1 mm and (*b*) maximum error as function of *l* for $\phi=50$ deg and $\theta=20$ deg

x_E, y_E, and z_E, and each of the corresponding inputs ρ_i $(i=1,2,3)$ by using Eq. (16) and Eqs. (9)–(11) and (14), respectively. Then, we sweep ϕ between $\phi-\phi_P$ and $\phi+\phi_P$, θ between $\theta-\theta_P$ and $\theta+\theta_P$, and z between $z-\varepsilon$ and $z+\varepsilon$ (where ϕ_P and θ_P are sufficiently large) and for each pose find the corresponding inputs $\rho_{i\varepsilon}$ using Eqs. (9)–(11) and (14). Only the poses for which all corresponding $\rho_{i\varepsilon}$ belong to $[\rho_i-\varepsilon,\rho_i+\varepsilon]$ will be retained. For each retained pose, the corresponding position coordinates x'_E, y'_E, and z'_E are calculated and the distance $E_N E_N^e$ is computed. Finally, the maximal value of this distance is retained, which will be E_e. Obviously, the maximum error of both tool heads is independent of the z value, and the error is proportional to the parameter l.

Figure 8(*a*) illustrates the relationship between the maximum error E_e and the orientation (ϕ,θ) of the mobile platform of a 3-$\underline{P}_V P_H S$ tool head when $\varepsilon=10$ μm, and $l=1$ mm. It shows that the larger the tilt angle θ the larger the error of point E, that the maximum error is always larger than the maximum input error ε. Figure 8(*b*) gives the relationship between the maximum error E_e and the length parameter l for a specified orientation $(\phi=50$ deg, $\theta=20$ deg). It indicates that the larger the length l, the larger this error for a certain orientation.

6 Dimensional Optimization

As is well known, the performance of a mechanism is strongly related to its geometrical parameters. Dimensional optimization is the process of determining the parameters required to enable the mechanism to achieve better relative performance.

6.1 The 3-$\underline{P}_V P_H S$ Tool Head. The analysis of the 3-$\underline{P}_V P_H S$ tool head shows that there is only one parameter, i.e., r, that should be optimized; the maximum pitch angle of the spherical joint in the mechanism is always equal to the tilt angle θ; the

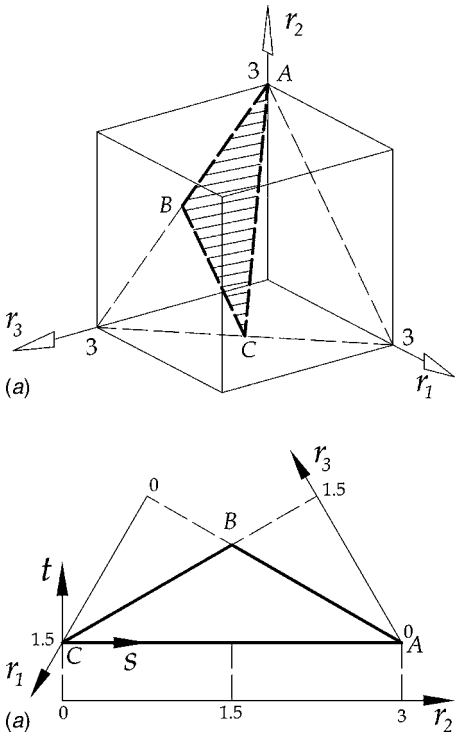

Fig. 9 Proposed parameter design space for the 3-$\underline{P}_V$RS tool head

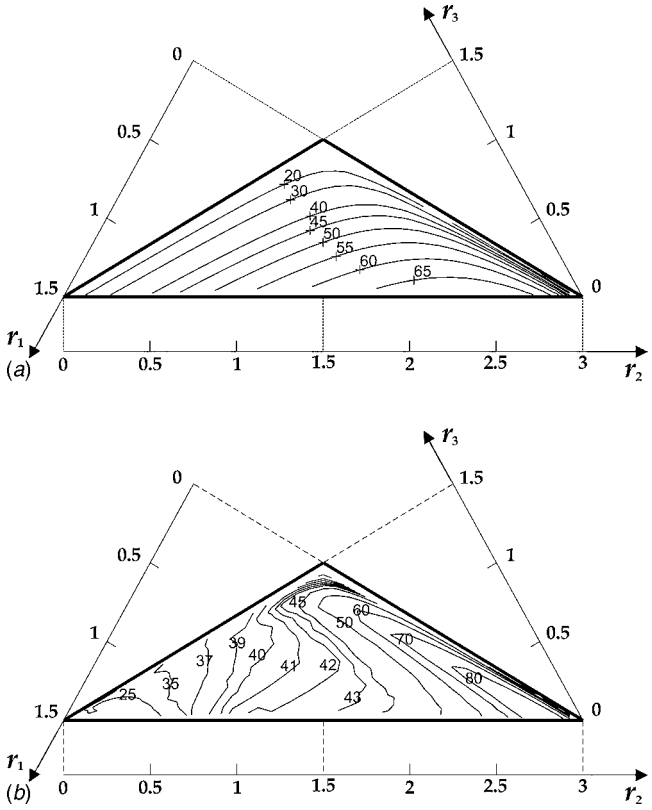

Fig. 10 Atlases for a 3-$\underline{P}_V$RS tool head: (*a*) orientation capability index (OCI) and (*b*) error index

maximum error of the point E is proportional to the tilt angle θ; and the error is proportional to the parameter r. Therefore, dimensional optimization of the tool head with respect to the orientation capability and output error of point E is trivial. The designer should simply select a desired tilt angle θ based on the maximum error index shown in Fig. 8(*a*) and determine the parameter r considering the actual application.

6.2 The 3-$\underline{P}_V$RS Tool Head. Since we have three dimensional parameters, r, L, and R, to be optimized for the 3-$\underline{P}_V$RS tool head, dimensional optimization of the mechanism is more difficult. As a performance atlas can visually show the relationship between performance and the design parameter(s), it is very useful in machine design and appears in most design manuals. Here, we extend the design concept introduced in [11] to the tool head. The first step is to develop a *parameter design space*.

6.2.1 Parameter Design Space. For the 3-$\underline{P}_V$RS tool head studied here, there are three geometric parameters, r, L, and R, which are all measured in length units. Note that each of the three parameters can have any value between zero and infinity. The greatest challenge is to develop a design tool that can embody all mechanism designs within a finite space.

For this reason, we must eliminate the physical link size [11], as follows. Let

$$D = \frac{r + L + R}{3} \tag{21}$$

Then, obtain three nondimensional parameters

$$r_1 = \frac{r}{D}, \quad r_2 = \frac{L}{D}, \quad \text{and} \quad r_3 = \frac{R}{D} \tag{22}$$

yielding

$$r_1 + r_2 + r_3 = 3 \tag{23}$$

This process makes it possible to reduce a three-dimensional problem to a two-dimensional one. Theoretically, the three nondimensional parameters r_1, r_2, and r_3 can have any value between 0 and 3. For the parallel mechanism studied here, the three parameters should be

$$0 < r_1, r_2, r_3 < 3, \quad r_1 \le r_3, \quad \text{and} \quad r_1 + r_2 > r_3 \tag{24}$$

Based on Eqs. (23) and (24), a *parameter design space* can be established as shown in Fig. 9(*a*), in which the triangle ABC is actually our target. In Fig. 9(*a*), this triangle is restricted by r_1, r_2, and r_3. However, it can take another form, as shown in Fig. 9(*b*), which is called the planar-closed configuration of the parameter design space. This configuration makes it easier for us to plot an atlas.

For convenience, two orthogonal coordinates s and t are utilized to express r_1, r_2, and r_3. Thus, by using

$$\begin{cases} s = r_2 \\ t = \sqrt{3} - \dfrac{2r_1}{\sqrt{3}} - \dfrac{r_2}{\sqrt{3}} \end{cases} \tag{25}$$

coordinates, r_1, r_2, and r_3 can be transformed into s and t, making Eq. (25) useful for constructing an atlas.

6.2.2 Atlases of Orientation Capability and Error Indices. The *orientation capability index* (OCI) is defined as the maximum tilt angle that can be achieved in any direction (for any ϕ), i.e., the minimum of the orientation capability. For example, the OCI of the 3-$\underline{P}_V$RS studied in Sec. 4.3 is 56 deg (see Fig. 6). However, to avoid crossing a singularity due to the input errors, our OCI does not represent the angle from the actual singular orientation, but rather from the smallest orientation from which input errors can lead the mechanism to a singular configuration.

The atlas illustrating the relationship between the normalized parameters r_i $(i=1,2,3)$ and the OCI is shown in Fig. 10(*a*), from which we can see that the index is inversely proportional to the

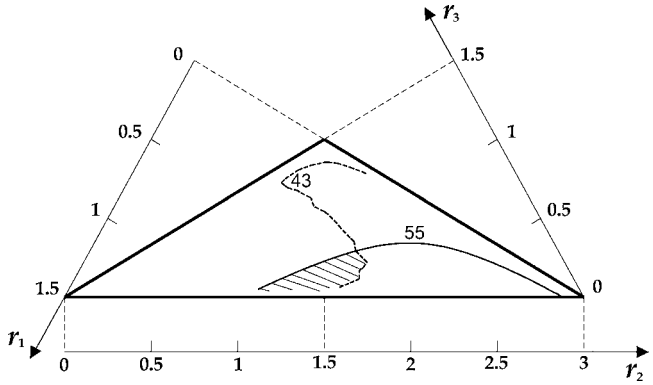

Fig. 11 An identified optimum region when OCI >55 deg and $E_{e\_max}<43$ μm

parameter r_3.

For comparison purposes, the error index is defined as the largest value, denoted as E_{e_max}, of all maximum errors E_e of point E at the z-axis when $\varepsilon=10$ μm, $\phi\in[-90\text{ deg},90\text{ deg}]$ and $\theta\in[-\text{OCI},\text{OCI}]$. Letting $l=1$, Fig. 10(*b*) shows the atlas of the error index, from which we can see that a smaller r_2 usually leads to poorer accuracy.

6.2.3 Optimization Process. Supposing that an application needs the tool head to have a desired orientation capability of 40 deg about any axis in the *o-xy* plane and higher accuracy, the optimization process based on the atlases in Fig. 10 can be summarized as follows.

Step 1. Identify an optimum region in the parameter design space. According to the definition of OCI, some orientations that are near singularity will cause the mechanism to be out of control, and the accuracy near them to be poorer. This means that, if we use the desired orientation capability to find a mechanism in the atlas of Fig. 10(*a*), then the tool head will be unable to reach that capability in practice. For this reason, to identify an optimum region, we use the constraint OCI >55 deg (we allow a 15 deg safety buffer). For the error, $E_{e\_max}<43$ μm is defined as the error constraint. With the OCI and error constraints, an optimum region, denoted $\Omega_{\text{OCI}-E}$, can be identified (shown as the hatched region in Fig. 11) using the atlases in Fig. 10. The optimum region contains all possible solutions with the parameters r_i $(i=1,2,3)$ that are subject to the design requirement.

Step 2. Select a solution candidate from the optimum region. This region contains all possible solutions for the design. Since there is no best solution, but only a comparatively better one, we can pick any nondimensional mechanism from this region. For example, the mechanism with $r_1=0.65$, $r_2=1.5$, and $r_3=0.85$. The OCI and the error index E_{e_max} of this mechanism are 58.55 deg and 42.5 μm respectively.

Step 3. Determine the dimensional parameters r, L, and R. According to Eq. (22), we first need to determine the normalization factor D. As described in [11], this factor can be obtained by comparing the desired workspace of a design problem to the workspace of the nondimensional mechanism selected from the optimum region. For the 3-$\underline{\text{P}}_{\text{V}}$RS tool head considered here, any performance is independent of the positional workspace along the z-axis, and the orientation workspace is dependent on the ratio of related linear parameters, but not on any one parameter. Therefore, we cannot determine factor D with respect to the orientation workspace. In this case, we first need to determine the parameter r according to the practical application, and let the parameter be as small as possible in order to reduce the size of the mechanism. Here, we suppose that $r=200.00$ mm. Then, we have $D=r/r_1=200/0.65\approx307.70$ mm. Accordingly, we get $L=Dr_2\approx461.55$ mm and $R=Dr_3\approx261.55$ mm.

Step 4. Check the error of the dimensional mechanism, and, if necessary, revise the design solution. In the previous step, we determined the dimensional parameters, which are $r=200.00$ mm, $L=461.55$ mm, and $R=261.55$ mm. In this step, we must check the error/accuracy of the solution for the desired orientation capability. Before doing so, however, we need to determine the distance l between the point E and o. We can suppose that point E is the end point of the tool mounted on the mobile platform. In our design problem, the desired orientation capability is 40 deg. For $\phi\in[-90\text{ deg},90\text{ deg}]$ and $\theta\in[-40\text{ deg},40\text{ deg}]$, numerical calculations show that the error index E_{e_max} of point E for the input error $\varepsilon=10$ μm is 9.0 μm if $l=100$ mm. If the error is acceptable, we proceed to step 5. If the error is greater than expected, we return to step 2, pick up another group of nondimensional parameters from the optimum region with a smaller error, and repeat steps 3 and 4. This design method allows the designer to adjust his/her design solution, which is the advantage of the approach.

Step 5. Calculation of the input range. The input range required to reach the orientation capability of 40 deg can be calculated using Eq. (14). For the solution obtained in step 4, we have $\rho_i=[-570.9079\text{ mm},-313.7929\text{ mm}]$ $(i=1,2,3)$ when $z=0$. The final input range for each actuator should include the positional workspace along the z-axis.

Note that, if the input range does not correspond to an off-the-shelf actuator, the designer can return to step 2 and pick up another nondimensional mechanism to adjust the design, or return to step 1 and identify another optimum region.

For comparison purposes, letting $r=200.00$ mm, $z=0$ and $l=100$ mm, the error index E_{e_max} of point E in the z-axis of the 3-$\underline{\text{P}}_{\text{V}}\text{P}_{\text{H}}$S tool head for the input error $\varepsilon=10$ μm is 10.0 μm. The input range for the same orientation capability when $z=0$ is $[-128.5575\text{ mm},128.5575\text{ mm}]$. We can see that the accuracy of the 3-$\underline{\text{P}}_{\text{V}}$RS tool head is somewhat high, while the actuated lengths of the inputs for the two mechanisms are almost the same. This means that, although the optimal design of the 3-$\underline{\text{P}}_{\text{V}}$RS tool head is more difficult than that of the 3-$\underline{\text{P}}_{\text{V}}\text{P}_{\text{H}}$S too head, the accuracy of the 3-$\underline{\text{P}}_{\text{V}}$RS tool head can be improved by dimensional optimization.

7 Conclusions

This paper addresses the issues of orientation capability and error/accuracy analysis and dimensional optimization of the 3-$\underline{\text{P}}_{\text{V}}\text{P}_{\text{H}}$S and 3-$\underline{\text{P}}_{\text{V}}$RS tool heads. Our analysis and optimization lead us to the following conclusions:

1. The orientation capability and error/accuracy indices of both tool heads are independent of the positional workspace, i.e., z. This is very important for the design and application of the tool heads.
2. The orientation capability of the two tool heads can be more than ±40 deg.
3. The accuracy becomes poorer when the tilt angle θ of the mobile platform is increased.
4. The dimension synthesis of the 3-$\underline{\text{P}}_{\text{V}}\text{P}_{\text{H}}$S tool head is very simple. All the designer needs to do is select a desired tilt angle θ based on the maximum error index shown in Fig. 8 and determine the size of the mobile platform considering the practical application. Thus, the performance of the 3-$\underline{\text{P}}_{\text{V}}\text{P}_{\text{H}}$S tool head cannot be improved by dimensional optimization.
5. The dimensional optimization of the 3-$\underline{\text{P}}_{\text{V}}$RS tool head is much more difficult; however, the accuracy of the tool head can be improved by using our method.
6. The optimization method used in this paper can find all the possible optimal solutions for a design problem of the 3-$\underline{\text{P}}_{\text{V}}$RS tool head.

The results of this paper will be useful for the development and

application of these two types of articulated tool head. Furthermore, the analysis and optimization methods introduced here can be extended to other parallel robots.

Acknowledgment

This work was supported by the Ministère de l'Éducation, du Loisir et du Sport du Québec, and partially by the National Natural Science Foundation of China under Grant No. 50505023 and the High Technology Research and Development Program (863 Program) of China (Grant No. 2006AA04Z227), and was carried out during a two-month visit by the first author to the École de technologie supérieure, Montreal, Canada, in the summer of 2006.

Nomenclature

$\mathfrak{R}$ = the base frame $O-XYZ$
$\mathfrak{R}'$ = the mobile frame $o-xyz$
P_i = centers of the mobile platform spherical joints
B_i = vertices of the active joints
θ = tilt angle, orientation capability of the mobile platform
ϕ = azimuth angle, $-90 \text{ deg} \leq \phi \leq 90 \text{ deg}$
ψ_i = angle between the restricting planes
$\boldsymbol{p}_i'$ = vectors of points P_i in frame $\mathfrak{R}'$
$\boldsymbol{p}_{i\mathfrak{R}}$ = vectors of points P_i in frame $\mathfrak{R}$
$\boldsymbol{R}_a(\theta)$ = rotation matrix about an a-axis defined by angle ϕ, which is measured between the x-axis (not the X-axis) and the a-axis
OCI = orientation capability index
D = the average of r, R and L
l = distance between points E on the mobile z-axis and o
$\mathbf{b}_{i\mathfrak{R}}$ = vectors of points B_i in frame $\mathfrak{R}$
R = the geometric parameter for the base platform
L = the length of each link P_iB_i
r_i = nondimensional geometric parameters
r = the radius of the mobile platform
$\tilde{\alpha}_v$ = absolute pitch angle of a spherical joint
α_v = pitch angle of a spherical joint
α_u = yaw angle of a spherical joint
D = the average of r, R, and L
l = distance between points E on the mobile z-axis and o

References

[1] Wahl, J., 2000, "Articulated Tool Head," WIPO Patent No. WO 00/25976.
[2] Fernandez, A. J. S., Jimenez, V. C., and Olazabal, M. G., 2002, "Kinematical System for a Movable Platform of a Machine," European Patent No. EP1245349(A1).
[3] Bonev, I. A., 2002, "Geometric Analysis of Parallel Mechanisms," Ph.D. thesis, Laval University, Quebec.
[4] Lee, K.-M., and Shah, D. K., 1988, "Kinematic Analysis of a Three-Degree-of-Freedom in-Parallel Actuated Manipulator," IEEE J. Rob. Autom. **4**(3), pp. 354–360.
[5] Carretero, J. A., Nahon, M. A., and Podhorodeski, R., 2000, "Workspace Analysis and Optimization of a Novel 3-DOF Parallel Manipulator," IEEE Trans. Rob. Autom., **15**(4), pp. 178–188.
[6] Pond, G. T., and Carretero, J. A., 2004, "Kinematic Analysis and Workspace Determination of the Inclined PRS Parallel Manipulator," *Proc. of 15th CISM-IFToMM Symposium on Robot Design, Dynamics, and Control*, Paper No. Rom04-18, Montreal.
[7] Liu, X.-J., Pruschek, P., and Pritschow, G., 2004, "A New 3-DOF Parallel Mechanism With Full Symmetrical Structure and Parasitic Motions," *Proc. of International Conf. on Intelligent Manipulation and Grasping*, Genoa, Italy, June, pp. 389–394.
[8] Gosselin, C., and Angeles, J., 1989 "The Optimum Kinematic Design of a Spherical Three-Degree-of-Freedom Parallel Manipulator," ASME J. Mech., Transm., Autom. Des., **111**(2), pp. 202–207.
[9] Ottaviano, E., and Ceccarelli, M., 2002, "Optimal Design of CaPaMan (Cassino Parallel Manipulator) With a Specified Orientation Workspace," Robotica, **20**, pp. 159–166.
[10] Chablat, D., and Wenger, P., 2003, "Architecture Optimization of a 3-DOF Parallel Mechanism for Machining Applications: The Orthoglide," IEEE Trans. Rob. Autom., **19**(3), pp. 403–410.
[11] Liu, X.-J., Wang, J., and Kim, J., 2006, "Determination of the Link Lengths for a Spatial 3-DoF Parallel Manipulator," ASME J. Mech. Des., **128**, pp. 365–373.
[12] Merlet, J. P., 2006, 'Jacobian, Manipulability, Condition Number, and Accuracy of Parallel Robots," ASME J. Mech. Des., **128**, pp. 199–206.
[13] Gosselin, C., and Angeles, J., 1991, "A Global Performance Index for the Kinematic Optimization of Robotic Manipulators," ASME J. Mech. Des., **113**, pp. 220–226.
[14] Liu, X.-J., Wang, J., and Pritschow, G., 2006, "Kinematics, Singularity and Workspace of Planar 5R Symmetrical Parallel Mechanisms," Mech. Mach. Theory **41**(2), pp. 145–169.